

High-order accurate thin layer approximations for time-domain electromagnetics.

Part I: General metal backed coatings

S. Chun

Division of Applied Mathematics
Brown University
Providence, RI 02912, USA
Sehun.Chun@Brown.edu

J. S. Hesthaven

Division of Applied Mathematics
Brown University
Providence, RI 02912, USA
Jan.Hesthaven@Brown.edu

May 6, 2008

Abstract

We present a family of high-order accurate thin layer approximations for time-domain electromagnetics. The thin layer approximations are valid for metal backed coatings of general isotropic materials and certain classes of anisotropic materials on smooth curvilinear backgrounds. Both dielectric and magnetic materials can be considered. The implementation of these models is non-trivial and we discuss this in the context of discontinuous Galerkin methods which are particularly well suited for these models. The range of validity, accuracy, and stability of the resulting schemes is demonstrated through one- and two-dimensional examples.

1 Introduction

Thin layer approximation, also known as approximate boundary conditions, are boundary conditions that model a thin layer which is not fully resolved. It was first used for ground wave propagation over the Earth during World War II although it has been known for more than 80 years. In 1940, S.M. Rytov [1] at the Institute of Physics at Russia, who sought an improvement of classical boundary condition of perfectly electric conductor (PEC), showed that the tangential

components of the electric field can be expressed as the tangential components of the magnetic field using the power series in terms of the thickness of a thin layer. Since then, it has been widely used and further developments are now studied [6]. To understand the objective of thin layer approximation, recall that we know the exterior field of an object considering the interior field of it. However, we can seek to compute the exterior field using a thin layer approximation at the boundary values of exterior field only. In other words, the problem with two different medium can be converted into a problem with a single medium and a complex boundary conditions. The importance comes from the efforts of eliminating computational constraints due to the thin layer. Computing without the need for small grids inside the thin layer significantly reduces the size of the discrete model and consequently reduces the computations, especially when the layer is thin compared to the wavelength of the incident wave. In this paper, high-order thin layer approximations for metal-backed coating are derived and studied in the context of discontinuous Galerkin method.

What remains is structured as follows. In Sec. 2 we sketch the derivation of the general family of effective boundary conditions for thin coatings. This sets the stage for Sec. 3 where we briefly introduce the discontinuous Galerkin methods for time-domain electromagnetics and discuss how the effective boundary conditions fit very well within this formulation. In Sec. 4 we consider the performance of the effective boundary conditions for several one-dimensional test cases to illustrate the behavior and convergence order of the thin coating models. This is extended in Sec. 5 to general the two-dimensional cases with curvilinear metallic backings and we also consider range of validity for thick coatings and the extension to problems with non-smooth metal backing. In Sec. 6 we summarize the results and discuss the extension to cases with multi-layer coatings and other generalizations.

2 Formulation of effective time-domain boundary conditions

Let us consider a general but smooth perfectly conducting scatterer in Ω and assume that it is coated with a thin homogeneous material layer of uniform thickness η as illustrated in Fig. 1. Let Ω^η represent the thin layer.

Assume that Γ^ν is the interface between the thin layer and the scatterer and that Γ is the interface between the thin layer and free space. We shall assume all boundaries are smooth but no other restrictions are imposed.

We introduce E^η , H^η as the electric and magnetic fields, respectively, and let $\hat{\varepsilon}^\eta$, $\hat{\mu}^\eta$ be the permittivity and permeability tensor in the thin layer Ω^η . Furthermore, in $\Omega^\nu (\equiv \Omega \setminus \Omega^\eta)$ we have E , H as the electric and magnetic fields and we let $\hat{\varepsilon}$, $\hat{\mu}$ be the permittivity and permeability tensors. Outside the scatterer we typically assume vacuum, although this is not required.

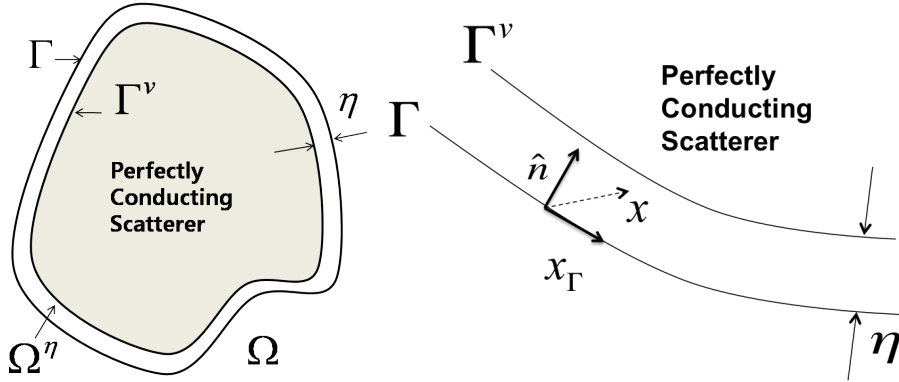


Figure 1: On the left we summarize the definitions of the domains and the boundaries and on the right we show the local coordinate system used along the smooth scatterer boundary.

Consider now the coupled system of Maxwell's equations

$$\hat{\epsilon} \frac{\partial E}{\partial t} - \nabla \times H = 0, \quad \hat{\mu} \frac{\partial H}{\partial t} + \nabla \times E = 0 \quad x \in \Omega \setminus \Omega^\eta \quad (1)$$

$$\hat{\epsilon}^\eta \frac{\partial E^\eta}{\partial t} - \nabla \times H^\eta = 0, \quad \hat{\mu}^\eta \frac{\partial H^\eta}{\partial t} + \nabla \times E^\eta = 0 \quad x \in \Omega^\eta \quad (2)$$

with the boundary conditions

$$E^\eta \times \hat{n} = 0, \quad x \in \Gamma^\nu \quad (3)$$

$$E \times \hat{n} = E^\eta \times \hat{n}, \quad H \times \hat{n} = H^\eta \times \hat{n}, \quad x \in \Gamma, \quad (4)$$

where \hat{n} represents the outward pointing normal vector. Under the assumption of a constant layer thickness, \hat{n} is taken to be the same on Γ and Γ^ν . Assume now that the layer, Ω^η , is thin compared to a characteristic wavelength of the sources. In this case the two systems of equations, Eqs. (1)-(2), have very different scales introduced by the geometry which would cause computational difficulties.

Let us therefore seek to construct an effective boundary conditions on Γ of the form

$$E \times \hat{n} = \mathfrak{B}^k(\hat{n} \times (H \times \hat{n})), \quad x \in \Gamma.$$

Here \mathfrak{B}^k represents the effective conditions and connects the field components at the interface through a scheme which mimics the presence of the thin coating. The parameter k reflects a hierarchy of conditions of increasing order of accuracy. If we are successful in deriving such a model, we can apply these effective boundary conditions to the exterior system, Eq. (1), to model the impact of the thin coating through the effective boundary condition.

We express the point x inside Ω^η as

$$x = x_\Gamma + s\hat{n} = x_\Gamma + \eta\nu\hat{n}, \quad x_\Gamma \in \Gamma, \nu \in [0, 1]$$

where we assume that the layer has a constant thickness and is homogeneous. Recall that \hat{n} can vary along the curve. Under the thin layer assumption we then make the formal approximation through the expansion of E^η and H^η as

$$\begin{aligned} E^\eta(x, t) &= E_0(x_\Gamma, \nu, t) + \eta E_1(x_\Gamma, \nu, t) + \eta^2 E_2(x_\Gamma, \nu, t) + \dots \\ H^\eta(x, t) &= H_0(x_\Gamma, \nu, t) + \eta H_1(x_\Gamma, \nu, t) + \eta^2 H_2(x_\Gamma, \nu, t) + \dots \end{aligned} \quad (5)$$

Note in particular that E_k and H_k are both independent of η and depends only on the position x_Γ along the boundary and the normalized position ν in the layer.

Along the general layer surface x_Γ , the differential operator ∇ is

$$\nabla = \nabla_\Gamma + \frac{1}{\eta} \frac{\partial}{\partial \nu},$$

and the corresponding curl operator $\nabla \times$ takes the form (see [2] for a detailed proof)

$$\nabla \times V = \mathcal{T}_\Gamma^s V - \frac{1}{\eta} \frac{\partial}{\partial \nu} (V \times \hat{n}),$$

for the generic vector field V . Here

$$\mathcal{T}_\Gamma^s V = [(\mathcal{R}_s \nabla_\Gamma) \cdot (V \times \hat{n})] \hat{n} + [\mathcal{R}_s \nabla_\Gamma (V \cdot \hat{n})] \times \hat{n} - (\mathcal{R}_s \mathcal{C} V) \times \hat{n}$$

and we have the curvature tensor, $\mathcal{C} = \vec{\nabla} \hat{n}$ and $\mathcal{R}_s(\Pi_{||} + s\mathcal{C}) = \Pi_{||}$ is the projection operator along the tangential direction of Γ . Inserting this into Eq. (2), we obtain

$$\begin{aligned} \hat{\varepsilon}^\eta \frac{\partial E^\eta}{\partial t} - \mathcal{T}_\Gamma^s H^\eta + \frac{1}{\eta} \frac{\partial}{\partial \nu} (H^\eta \times \hat{n}) &= 0, & x \in \Omega^\eta \\ \hat{\mu}^\eta \frac{\partial H^\eta}{\partial t} + \mathcal{T}_\Gamma^s E^\eta - \frac{1}{\eta} \frac{\partial}{\partial \nu} (E^\eta \times \hat{n}) &= 0. \end{aligned} \quad (6)$$

We then assume the validity of the expansion

$$\mathcal{R}_s = \Pi_{||} + \sum_{i=1}^{\infty} (-\eta\nu\mathcal{C})^i,$$

to obtain the expansion of \mathcal{T}_Γ^s as

$$\mathcal{T}_\Gamma^s = \sum_{i=0}^{\infty} (-s)^i \mathcal{T}_\Gamma^i \quad (7)$$

where

$$\mathcal{J}_\Gamma^i V = [(\mathcal{C}^i \nabla_\Gamma) \cdot (V \times \hat{n})] \hat{n} + [\mathcal{C}^i \nabla_\Gamma (V \cdot \hat{n})] \times \hat{n} - (\mathcal{C}^{i+1} V) \times \hat{n}.$$

Substituting Eqs. (5) and (7) into Eq. (6), we obtain the following hierarchy of equations for $k = 0, 1, 2, \dots$

$$\begin{aligned} \hat{\varepsilon}^\eta \frac{\partial E_k}{\partial t} - \sum_{i=1}^k (-\nu)^i \mathcal{J}_\Gamma^i H_{k-i} + \frac{\partial}{\partial \nu} (H_{k+1} \times \hat{n}) &= 0 \quad x \in \Omega^\eta \quad (8) \\ \hat{\mu}^\eta \frac{\partial H_k}{\partial t} + \sum_{i=1}^k (-\nu)^i \mathcal{J}_\Gamma^i E_{k-i} - \frac{\partial}{\partial \nu} (E_{k+1} \times \hat{n}) &= 0. \end{aligned}$$

subject to the boundary conditions

$$\begin{aligned} \hat{n} \times E_{k+1}(x_\Gamma, 1, t) &= 0, \quad (9) \\ \hat{n} \times H_{k+1}(x_\Gamma, 0, t) &= \hat{n} \times H_{k+1}(\Gamma). \end{aligned}$$

Solving Eqs. (8)-(9) up to k leads to an $(k+1)$ 'th order of effective boundary conditions (EBC) which can be used to supply boundary conditions to the exterior Maxwell's equations, Eq. (1).

The effective boundary condition of order 2 becomes

$$\frac{\partial E}{\partial t} \times \hat{n} = -\eta \hat{\mu}^\eta \frac{\partial^2 \varphi}{\partial t^2} - \eta (\hat{\varepsilon}^\eta)^{-1} \vec{\nabla}_\Gamma \times (\nabla_\Gamma \times \varphi), \quad x \in \Gamma \quad (10)$$

and the third order condition is

$$\begin{aligned} \frac{\partial E}{\partial t} \times \hat{n} &= -\eta \hat{\mu}^\eta [1 - \eta(\mathcal{C} - \mathcal{H})] \frac{\partial^2 \varphi}{\partial t^2} \\ &\quad - \eta (\hat{\varepsilon}^\eta)^{-1} \vec{\nabla}_\Gamma \times [1 - \eta \mathcal{H}] (\nabla_\Gamma \times \varphi), \quad x \in \Gamma \quad (11) \end{aligned}$$

Here $\varphi = \Pi_{\parallel} H = \hat{n} \times (H \times \hat{n})$ and

$$\vec{\nabla}_\Gamma \times V = (\nabla_\Gamma V) \times \hat{n}, \quad \nabla_\Gamma V = \nabla_\Gamma \cdot (V \times \hat{n}),$$

and $\mathcal{H} = \frac{1}{2} \text{tr} \mathcal{C}$ is the mean Gaussian curvature.

The general approach can be continued although the expressions become increasingly complex. A fourth order effective boundary condition for planar boundaries is given as

$$\begin{aligned} \frac{\partial E}{\partial t} \times \hat{n} &= -\eta \hat{\mu}^\eta \frac{\partial^2 \Psi}{\partial t^2} - \eta (\hat{\varepsilon}^\eta)^{-1} \vec{\nabla}_\Gamma \times (\nabla_\Gamma \times \Phi) \quad x \in \Gamma \quad (12) \\ \Phi + \frac{\eta^2}{3} \vec{\nabla}_\Gamma \times (\nabla_\Gamma \times \Phi) &= \varphi \\ \Psi + \frac{\eta^2}{3} \left(\bar{\varepsilon}^\eta \hat{\mu}^\eta \frac{\partial^2 \Psi}{\partial t^2} - \bar{\Delta}_\Gamma \Psi + \vec{\nabla} \times (\nabla \times \Psi) \right) &= \varphi, \end{aligned}$$

where $\bar{\varepsilon}^\eta = \text{tr} \hat{\varepsilon}^\eta - \hat{\varepsilon}^\eta$ and

$$\Delta_\Gamma V = \nabla_\Gamma (\nabla_\Gamma \cdot V) - \vec{\nabla}_\Gamma \times (\nabla_\Gamma \times V).$$

3 Time-domain scheme using a discontinuous Galerkin method

The efficient boundary conditions discussed above have to be solved along with the free-space Maxwell's equations, given in Eq. (1). Since the main interest is in problems with geometrically complex coated scatterer illuminated by time-dependent sources, a body conforming time-domain formulation is most natural and classic finite-difference time-domain schemes [4] are of less interest. Furthermore, since the goal here is to demonstrate the high-order accuracy of the efficient boundary conditions, it is essential that a high-order accurate scheme be considered.

Based on these observations, it is natural to consider a discontinuous Galerkin method [5] which has been developed during the last decade and has shown great promise as a flexible, accurate, and robust way to solve the time-domain Maxwell's equations [3].

Let us briefly sketch the derivation of the discontinuous Galerkin scheme for the time-domain Maxwell's problem. We begin by assuming that the computational vacuum domain, Ω^v , is approximated by K elements D^k as

$$\Omega^v \simeq \sum_{k=1}^K D^k$$

where we assume that D^k are d -dimensional simplices.

In each of these elements we assume that E and H can be approximation by Lagrange polynomials (ℓ_j) as

$$[E_h, H_h] = \sum_{j=1}^N [E(x_j, t), H(x_j, t)] \ell_j(x),$$

where x_j are the interpolation points on which the Lagrangian basis is based. The number of terms N in the expansion is given as

$$N = \binom{n+d}{n}$$

for the n 'th order polynomial in d -dimensions. For details of how this local interpolation is recovered we refer to [5].

To derive the scheme, we insert the approximate solution into Maxwell's equations and require that the local residual is orthogonal to all n 'th order polynomials. Integration by parts twice this yields the scheme

$$\begin{aligned} \int_{\mathbb{D}^k} (\hat{\epsilon} \frac{\partial E_h}{\partial t} - \nabla \times H_h) \ell_i(x) dx &= - \int_{\partial \mathbb{D}^k} \hat{n}^k \times (H_h - H^*) \ell_i(x) dx \\ \int_{\mathbb{D}^k} (\hat{\mu} \frac{\partial H_h}{\partial t} + \nabla \times E_h) \ell_i(x) dx &= \int_{\partial \mathbb{D}^k} \hat{n}^k \times (E_h - E^*) \ell_i(x) dx \end{aligned}$$

where $[E^*, H^*]$ indicates the numerical flux of the corresponding vector quantity and \hat{n}^k reflects the outward pointing normal vector along ∂D^k . It is the numerical flux which is responsible for the coupling of the elements, for the stability of the scheme, and the imposition of boundary conditions.

Enforcing the effective boundary conditions is done though the numerical flux for those elements sharing a face with Γ as

$$\begin{aligned} \int_{\mathbb{D}^k} (\hat{\varepsilon} \frac{\partial E_h}{\partial t} - \nabla \times H_h) \ell_i(x) dx &= - \int_{\partial \mathbb{D}^k \setminus \Gamma} \hat{n}^k \times (H_h - H^*) \ell_i(x) dx \\ &\quad - \oint_{\Gamma} \hat{n}^k \times (H_h - H_\varphi^\eta) \ell_i(x) dx \\ \int_{\mathbb{D}^k} (\hat{\mu} \frac{\partial H_h}{\partial t} + \nabla \times E_h) \ell_i(x) dx &= \int_{\partial \mathbb{D}^k \setminus \Gamma} \hat{n}^k \times (E_h - E^*) \ell_i(x) dx. \end{aligned}$$

where H_φ^η is defined through $\varphi = \hat{n} \times (H_\varphi^\eta \times \hat{n})$ and φ is obtained from the effective boundary conditions. Note also that $\int_{\Gamma} (\hat{n} \times (E_h - E^*) \ell_i(x)) dx = 0$, since we assume tangential continuity of E across the coating interface through $E_h = E^*$ along Γ .

To connect the elements away from the boundary we use a central flux as

$$E^* = \frac{1}{2} (E_h^- + E_h^+), \quad H^* = \frac{1}{2} (H_h^- + H_h^+),$$

where E_h^- refers to the interior solution and E_h^+ is the exterior solution. Other flux choices are possible and an extensive discussion can be found in [5].

4 One dimensional coatings

Let us first consider the one-dimensional case and assume that z is the direction of wave propagation. In this case the three-dimensional Maxwell's equations separate into two systems of tangential components with $E = [E_x, E_y]^T$ and $H = [H_x, H_y]^T$ on the form

$$\hat{\varepsilon} \frac{\partial E}{\partial t} = \hat{\sigma} \frac{\partial H}{\partial z}, \quad \hat{\mu} \frac{\partial H}{\partial t} = -\hat{\sigma} \frac{\partial E}{\partial z}, \quad \hat{\sigma} = \begin{bmatrix} 0 & -1 \\ 1 & 0 \end{bmatrix}.$$

In this simple case, the 2nd/3rd order effective boundary conditions are the same due to the planar boundary. They both reduce to

$$\frac{d\varphi}{dt} = \frac{1}{\eta} \hat{\sigma} E,$$

while the 4th/5th order effective boundary condition becomes

$$\frac{d\Phi}{dt} = \frac{1}{\eta} \hat{\sigma} E, \quad \Phi + \frac{\eta}{3} \hat{\varepsilon}^\eta \frac{\partial^2 \Phi}{\partial t^2} = \varphi$$

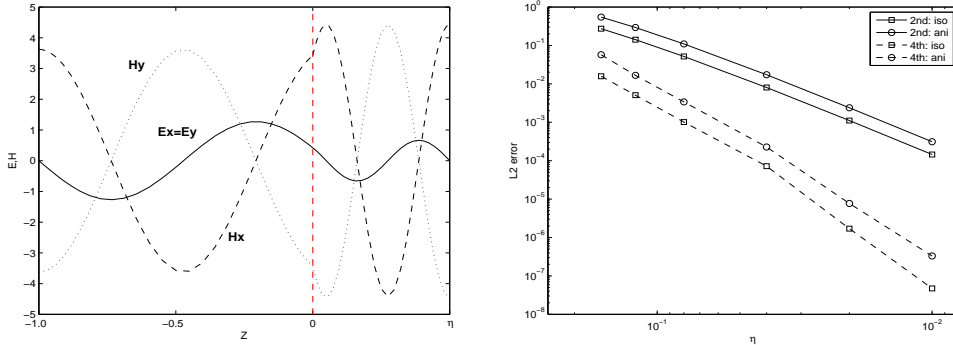


Figure 2: Initial condition for the cavity test case (left) and the convergence result (right) for the coated cavity problem. The solid line is the 2nd/3rd order effective boundary condition and the dashed line represents the 4th/5th order approximation. Squares are for an isotropic coating material with $\varepsilon^\eta = 2.25$ and circles represent an anisotropic coating material with $\varepsilon_{xx}^\eta = \varepsilon_{yy}^\eta = 4.0$, $\varepsilon_{xy}^\eta = \varepsilon_{yx}^\eta = 1.5$. The L_2 -error is measured at $T = \pi$.

where, $\bar{\varepsilon}^\eta = \text{tr } \hat{\varepsilon}^\eta - \hat{\varepsilon}^\eta$.

For the 2nd and 3rd order scheme, any explicit or implicit scheme can be used for the time marching. An implicit scheme is needed for the 4th order scheme, since φ is not explicitly expressed as a function of the fields. However, only the element containing Γ need to be used for the implicit scheme, so the computational impact of this is minimal.

4.1 Internally coated cavity

We consider an one-dimensional electromagnetic cavity with perfectly conducting walls located at $z^{(1)} = -1$ and $z^{(2)} = \eta$ as illustrated in Fig. 2. The interior of the cavity is filled with two dielectric media with the material interface at $z = 0$.

We consider the following general model

$$\begin{aligned} \begin{bmatrix} \varepsilon_{xx} & \varepsilon_{xy} \\ \varepsilon_{yx} & \varepsilon_{yy} \end{bmatrix} \frac{\partial}{\partial t} \begin{bmatrix} E_x \\ E_y \end{bmatrix} &= \begin{bmatrix} 0 & -1 \\ 1 & 0 \end{bmatrix} \frac{\partial}{\partial z} \begin{bmatrix} H_x \\ H_y \end{bmatrix} \\ \frac{\partial}{\partial t} \begin{bmatrix} H_x \\ H_y \end{bmatrix} &= - \begin{bmatrix} 0 & -1 \\ 1 & 0 \end{bmatrix} \frac{\partial}{\partial z} \begin{bmatrix} E_x \\ E_y \end{bmatrix} \end{aligned}$$

reflecting a general anisotropic dielectric material but no magnetic effects. The boundary conditions are given as

$$\text{i) } E = 0 \quad \text{or} \quad \frac{\partial H}{\partial z} = 0, \quad \text{at } z = -1, \eta$$

for the perfectly electrically conducting walls, and

$$\text{ii) } E^{(1)} = E^{(2)}, \quad H^{(1)} = H^{(2)}, \quad \text{at } z = 0,$$

to ensure tangential continuity across the material interface.

The solution of Maxwell's equations in this arrangement can be expressed as ($k = 1, 2$)

$$\begin{aligned} E_x^{(k)} &= [A^{(k)} e^{in^{(k)}\omega z} - B^{(k)} e^{-in^{(k)}\omega z}] e^{i\omega t} \\ E_y^{(k)} &= [A^{(k)} e^{in^{(k)}\omega z} - B^{(k)} e^{-in^{(k)}\omega z}] e^{i\omega t} \\ H_x^{(k)} &= n^{(k)} [A^{(k)} e^{in^{(k)}\omega z} + B^{(k)} e^{-in^{(k)}\omega z}] e^{i\omega t} \\ H_y^{(k)} &= -n^{(k)} [A^{(k)} e^{in^{(k)}\omega z} + B^{(k)} e^{-in^{(k)}\omega z}] e^{i\omega t} \end{aligned}$$

where

$$\begin{aligned} A^{(1)} &= \frac{n^{(2)} \cos(\eta n^{(2)} \omega)}{n^{(1)} \cos(n^{(1)} \omega)}, & A^{(2)} &= e^{-i\omega(n^{(1)} + \eta n^{(2)})} \\ B^{(1)} &= A^{(1)} e^{-i2n^{(1)} \omega}, & B^{(2)} &= A^{(2)} e^{i2\eta n^{(2)} \omega} \\ n^{(k)} &= \sqrt{\varepsilon_{xx}^{(k)} + \varepsilon_{xy}^{(k)}} = \sqrt{\varepsilon_{yy}^{(k)} + \varepsilon_{xy}^{(k)}}, \end{aligned}$$

and we require $\varepsilon_{xx}^{(k)} = \varepsilon_{yy}^{(k)}$ for simplicity. Here ω is the solution to the equation

$$-n^{(2)} \tan(n^{(1)} \omega) = n^{(1)} \tan(\eta n^{(2)} \omega)$$

In Fig. 2 and Table 1 we illustrate the 2nd/3rd and 4th/5th order convergence of effective boundary conditions as a function of η , measured in terms of free-space wave lengths. Both for the isotropic and the more complex anisotropic case do we recover approximate design order convergence rates.

η	0.16	0.12	0.08	0.04	0.02	0.01
Isotropic material inside thin layer						
EBC	2.74e-01	1.42e-01	5.17e-02	8.03e-03	1.11e-03	1.45e-04
2nd/3rd	order	2.29	2.48	2.69	2.85	2.94
EBC	1.57e-02	5.07e-03	1.01e-03	7.20e-05	1.70e-06	4.73e-08
4th/5th	order	3.93	3.97	3.81	5.41	5.16
Anisotropic material inside thin layer						
EBC	5.47e-01	2.94e-01	1.10e-01	1.72e-02	2.39e-03	3.11e-04
2nd/3rd	order	2.16	2.43	2.67	2.85	2.94
EBC	5.73e-02	1.67e-02	3.40e-03	2.27e-04	7.69e-06	3.30e-07
4th/5th	order	4.29	3.92	3.91	4.88	4.54

Table 1: L_2 -convergence rates for the effective boundary condition (EBC) 2nd/3rd and 4th/5th order are shown for the test case shown in Fig. 2.

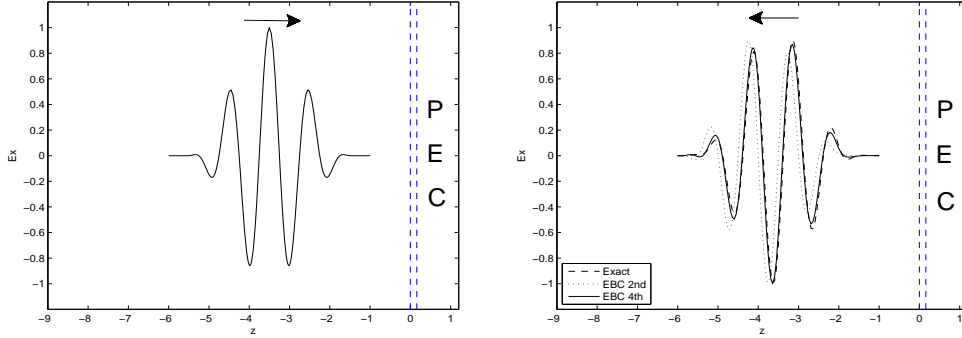


Figure 3: The initial condition of E_x (left) and the reflected value of E_x (right) from the brute-force computation with a thin layer of isotropic material (dashed line), from using a 2nd/3rd order effective boundary conditions (dotted line), and from using a 4th/5th order effective boundary condition (solid line). The thickness of the thin layer is $\eta = 0.16$ and the isotropic material is assume to have $\hat{\epsilon}^\eta = 1.5I$.

4.2 Comparison with brute-force computations

We consider the situation shown in Fig. 3 in which a general pulse impinges on a thinly coated metallic wall while on the left is a simple absorbing layer. A pulse is sent toward the coated surface and we compare the brute-force results – referred to as the ‘exact computation’ – with the results obtained by using the thin coating effective boundary conditions. In Fig. 3, the results obtained by using the 2nd/3rd order and the 4th/5th order effective boundary conditions are displayed. It is particularly noteworthy how much improvement there is in the accuracy of the phase error when increasing the order of the approximation. The left of Fig. 4 and Table 2 also confirms the expected convergence order of the effective boundary condition.

The real benefit of the effective boundary condition is found in the potential for a dramatically reduced computational time as compared to the brute-force computation using an explicit time marching scheme such as a Runge Kutta 4th order. For the brute-force approach, the stable timestep is proportional to η . In contrast to this, the stable timestep for the effective boundary condition shows no dependence of η as shown in Fig. 4. This yields a reduction in computational effort proportional to η^{-1} without compromising the accuracy.

5 Two-dimensional coatings

One of the unique features of the effective boundary conditions considered here is the ability to correctly account for curvature of the metallic backing. To explore this, let us consider the two-dimensional Maxwell’s equations for TE

η	0.20	0.16	0.12	0.08	0.04
Isotropic material inside thin layer					
EBC	2.41e-01	1.68e-01	8.48e-02	2.67e-02	3.19e-03
2nd/3rd	order	2.37	2.85	3.06	3.06
EBC	4.93e-02	2.43e-02	7.02e-03	9.20e-04	2.51e-05
4th/5th	order	4.31	5.01	5.20	5.10
Anisotropic material inside thin layer					
EBC	2.32e-01	1.94e-01	1.07e-01	3.21e-02	3.63e-03
2nd/3rd	order	2.08	2.97	3.15	3.08
EBC	8.35e-02	4.01e-02	1.42e-02	1.75e-03	4.22e-05
4th/5th	order	3.60	5.17	5.37	5.17

Table 2: L_2 -convergence rates for the effective boundary condition (EBC) of 2nd/3rd and 4th/5th order are shown for the test case shown in Fig. 3. The material properties of the isotropic material and the anisotropic materials are given as $\hat{\varepsilon}^\eta = 1.5I$ and $\varepsilon_{xx}^\eta = \varepsilon_{yy}^\eta = 1.5$, $\varepsilon_{xy}^\eta = \varepsilon_{yx}^\eta = 0.75$, respectively. The L_2 -error is measured at $T = 10.0$.

polarization in the (x, y) -plane

$$\begin{aligned}\hat{\varepsilon} \frac{\partial E}{\partial t} &= -\hat{\sigma} \nabla H_z \\ \hat{\mu} \frac{\partial H_z}{\partial t} &= (\nabla \times E) \cdot \hat{z}\end{aligned}$$

where $E = [E_x, E_y]^T$ and \hat{z} reflects a unit vector along the z -axis. In this polarization, the effective 2nd order boundary condition becomes

$$\left(\frac{\partial E}{\partial t} \times \hat{n} \right) \cdot \hat{z} = -\eta \mu^\eta \frac{\partial^2 \varphi_z}{\partial t^2} + \frac{\eta}{\varepsilon_r^\eta} \mu^\eta \frac{\partial^2 \varphi_z}{\partial x_\Gamma^2}, \quad x \in \Gamma,$$

where the general case reduces since $\varphi_z = H_z$. In the form of a system of equations,

$$\begin{aligned}(E \times \hat{n}) \cdot \hat{z} &= -\eta \mu^\eta \frac{\partial \varphi_z}{\partial t} - \eta \mu^\eta \frac{\partial \zeta_z}{\partial x_\Gamma} \\ \frac{\partial \zeta_z}{\partial t} &= -\frac{1}{\varepsilon_r^\eta} \frac{\partial \varphi_z}{\partial x_\Gamma}\end{aligned}$$

and $\frac{\partial}{\partial x_\Gamma}$ refers to differentiation along the surface of the coating Γ .

The 3rd order accurate effective boundary condition becomes

$$\left(\frac{\partial E}{\partial t} \times \hat{n} \right) \cdot \hat{z} = -\eta \mu^\eta [1 - \eta(\mathcal{C} - \mathcal{H}\mathcal{C})] \frac{\partial^2 \varphi_z}{\partial t^2} + \frac{\eta}{\varepsilon_r^\eta} \mu^\eta \frac{\partial}{\partial x_\Gamma} \left([1 - \eta \mathcal{H}\mathcal{C}] \frac{\partial \varphi_z}{\partial x_\Gamma} \right).$$

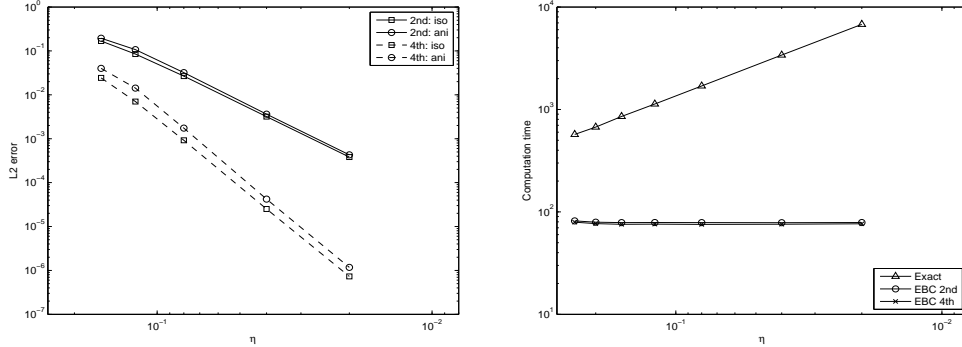


Figure 4: L_2 -error convergence rate (left) of 2nd/3rd order effective boundary condition for isotropic (solid line with squares) and anisotropic (solid line with circles) materials, and the results for the 4th/5th order effective boundary condition for isotropic(dashed line with squares), anisotropic (dashed line with circle) materials. Permittivity constants are $\hat{\varepsilon}^\eta = 1.5$ for the isotropic material and $\varepsilon_{xx}^\eta = \varepsilon_{yy}^\eta = 1.5$, $\varepsilon_{xy}^\eta = \varepsilon_{yx}^\eta = 0.75$ for the anisotropic material. On the right we show the computational time for the brute-force/exact computation (triangles), for the 2nd/3rd order effective boundary condition (circle), and for the 4th/5th order effective boundary condition (cross), showing the independence of the work on the thickness of the coating.

In the form of a system of equations,

$$\begin{aligned} (E \times \hat{n}) \cdot \hat{z} &= -\eta\mu^\eta[1 - \eta(\mathcal{C} - \mathcal{H})] \frac{\partial\varphi_z}{\partial t} - \eta\mu^\eta \frac{\partial\varphi_z}{\partial x_\Gamma} \\ \frac{\partial\zeta_z}{\partial t} &= -\frac{1}{\varepsilon_r^\eta}[1 - \eta\mathcal{H}] \frac{\partial\zeta_z}{\partial x_\Gamma}. \end{aligned}$$

Here, \mathcal{C} is the curvature tensor and \mathcal{H} is the mean curvature of the metallic backing for the coating. For an isotropic material, ε_r^η is simply a constant such that $\hat{\varepsilon}^\eta = \varepsilon_r^\eta I$ and for an anisotropic material it is a constant such that $(\hat{\varepsilon}^\eta E) \cdot \hat{n} = \varepsilon_r^\eta (E \cdot \hat{n})$, where $\hat{\varepsilon}^\eta$ indicates the permittivity tensor and I is the 2-identity matrix. This constraint naturally comes from the fact that the formulation is based on the separation of tangential and normal direction [2].

As a measure of accuracy, we use the radar cross section and generally compare the brute-force computation of this with the result obtained using the effective boundary condition. The radar cross section (RCS) is defined as [4]

$$\begin{aligned} F(\varphi) &\equiv \frac{e^{i(\pi/4)}}{\sqrt{8\pi k}} \oint_{C_a} \left[\omega\mu_0 \hat{z}' \cdot \check{J} - kz' \times \check{M}(r') \cdot \hat{r}' \right] e^{ik\hat{r} \cdot r'} dC \\ \text{RCS}(\varphi) &\equiv 2\pi \frac{|F(\varphi)|^2}{|E_{inc}|^2} \end{aligned}$$

where $\check{J} = \hat{n} \times H$ and $\check{M} = -\hat{n} \times E$ are the equivalent magnetic and electric currents on the surface C_a which completely encloses the scatterer. k and ω is the wave number and the frequency, respectively, of the illuminating plane wave; $r = R \cos \varphi$ is the far-field observation point and r' is the near-field source point in C_a .

5.1 Scattering by smooth coated cylinders

Let us first consider the most straightforward case of scattering by a two-dimensional cylinder with a smooth cross section. In this case, the derivation and assumptions of the effective boundary conditions are fulfilled and we should expect design order convergence.

5.1.1 Circular cylinder

We first consider a thinly-coated circular cylinder which is infinitely long along the z axis. Let R be the radius of the metallic cylinder and η be the constant thickness of the thin coating. Then, the curvature tensor is $\mathcal{C} = -\frac{1}{R+\eta}\tau$ and the mean curvature is $\mathcal{H} = -\frac{1}{2(R+\eta)}$, where τ is the tangential direction along the coating surface Γ .

In Fig. 5 we show the convergence of the RCS using the 2nd and 3rd order effective boundary condition. We note in particular the improved accuracy of the 3rd order condition for this case.

The actual convergence rates for the RCS are shown in Table 3 for both the 2nd and 3rd order effective boundary conditions for isotropic and anisotropic cases, showing close to design order accuracy when decreasing the thickness of the coating.

η	0.20	0.16	0.12	0.08	0.04
Isotropic material inside thin layer					
EBC 2nd	1.23e-01	8.24e-02	4.50e-02	1.82e-02	5.14e-03
order		1.27	1.78	2.21	2.37
EBC 3rd	1.12e-01	7.18e-02	3.36e-02	1.12e-02	1.08e-03
order		2.01	2.64	2.71	3.37
Anisotropic material inside thin layer					
EBC 2nd	1.22e-01	7.53e-02	3.86e-02	1.83e-02	5.13e-03
order		1.37	2.15	1.71	2.40
EBC 3rd	7.79e-02	5.05e-02	2.42e-02	8.38e-03	9.80e-04
order		1.94	2.56	2.61	3.10

Table 3: Convergence rate for the L_2 -error of the RCS for the 2nd and 3rd order effective boundary conditions (EBC) for the circular cylinder. Material constants are the same as given in Fig. 5.

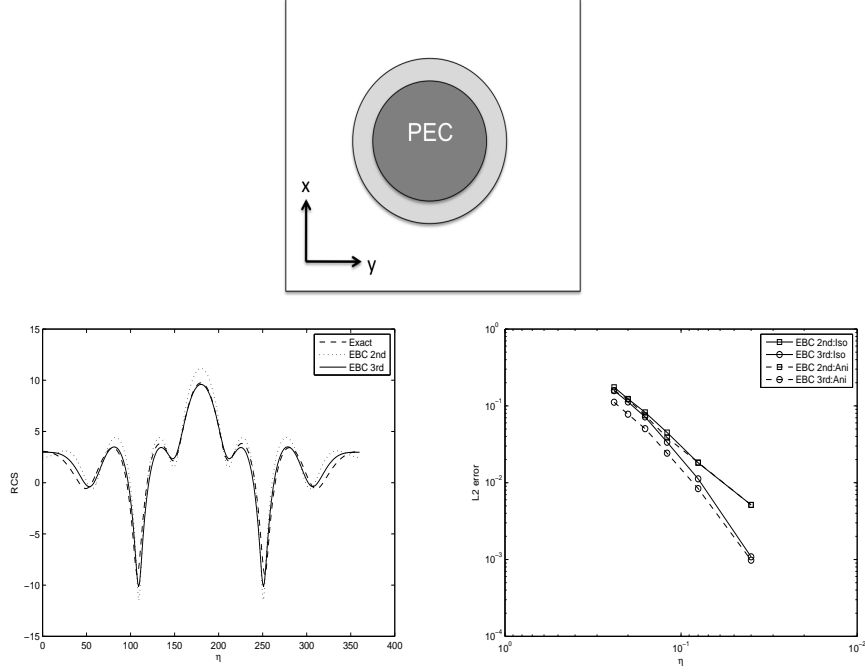


Figure 5: Radar cross section (RCS) of the brute force computation(dashed line), 2nd (dotted line) and 3rd (solid line) order effective boundary conditions for a circular cylinder with $\eta = 0.12\lambda$ are compared (left). λ is the wavelength of the incident wave. Also, L_2 -errors of the 2nd (square-solid line) and the 3rd (circle-solid line) order approximation for an isotropic material with $\varepsilon^\eta = 1.5$ and for an anisotropic materials with $\varepsilon_{xx}^\eta = \varepsilon_r^\eta n_x^2 + 1$, $\varepsilon_{xy}^\eta = \varepsilon_{yx}^\eta = \varepsilon_r^\eta n_x n_y$, $\varepsilon_{yy}^\eta = \varepsilon_r^\eta n_y^2 + 1$, $\varepsilon_r^\eta = 1.5$ are shown.

5.1.2 Elliptic cylinder

As a slightly more complex case, we consider a coated elliptic cylinder. Let a and b be the major and minor axis of the ellipsoid of the contour of Γ^v with the thickness of thin layer being η . Note that the contour of the interface $\partial\Omega$ at the distance of η from Γ^v in the normal direction is not an ellipsoid.

The curvature tensor is given as

$$\mathcal{C} = -\frac{ab}{(a^2 \cos^2 t + b^2 \sin^2 t)^{3/2}} \tau,$$

and the mean curvature is

$$\mathcal{H} = -\frac{ab}{2(a^2 \cos^2 t + b^2 \sin^2 t)^{3/2}},$$

where $t = \tan^{-1} \left(\frac{a}{b} \frac{y}{x} \right)$.

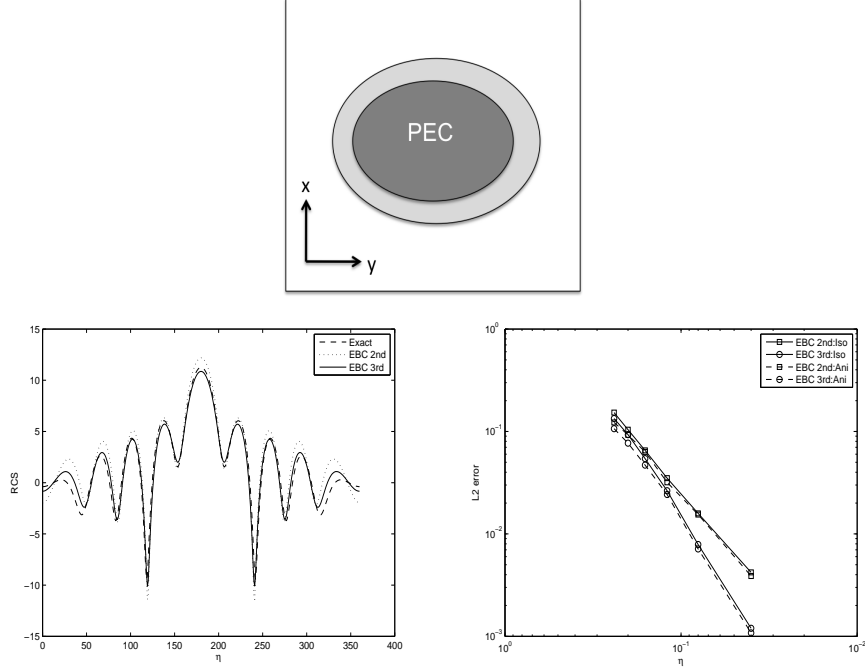


Figure 6: Radar cross section (RCS) of the brute force computation(dashed line), 2nd (dotted line) and 3rd (solid line) order effective boundary conditions for an elliptic cylinder with $\eta = 0.12\lambda$ are compared (left). λ is the wavelength of the incident wave. Major axis and minor axis of Γ is $(0.8 + \eta)\lambda$ and $(0.5 + \eta)\lambda$, respectively. Also, L_2 -errors of the 2nd (square-solid line) and the 3rd (circle-solid line) order approximation for isotropic material with $\varepsilon^\eta = 1.5$ for anisotropic materials with $\varepsilon_{xx}^\eta = \varepsilon_r^\eta n_x^2 + 1$, $\varepsilon_{xy}^\eta = \varepsilon_{yx}^\eta = \varepsilon_r^\eta n_x n_y$, $\varepsilon_{yy}^\eta = \varepsilon_r^\eta n_y^2 + 1$, $\varepsilon_r^\eta = 1.5$ are shown.

In Fig. 6 we show the convergence of the RCS when using the 2nd and 3rd order effective boundary condition. We note in particular the improved accuracy of the 3rd order condition for this case.

The actual convergence rates for the RCS is shown in Table 4 for both the 2nd and 3rd order effective boundary conditions for the isotropic and the anisotropic cases, confirming close to design order accuracy when the thickness of the coating is decreased.

5.2 Frequency dependence of the coating performance

While it is of primary interest to understand the performance of the thin coating approximation for very thin coatings, it is of practical importance to also understand when the approximation breaks down as the thickness of the layer increases.

η	0.20	0.16	0.12	0.08	0.04
Isotropic material inside thin layer					
EBC 2nd	1.04e-01	6.54e-02	3.51e-02	1.59e-02	4.21e-03
	order	1.04	1.32	2.00	2.36
EBC 3rd	9.32e-02	5.43e-02	2.64e-02	7.87e-03	1.20e-03
	order	2.41	2.51	2.98	2.72
Anisotropic material inside thin layer					
EBC 2nd	9.27e-02	6.31e-02	3.19e-02	1.54e-02	3.88e-03
	order	2.46	3.06	0.58	1.99
EBC 3rd	7.70e-02	4.69e-02	2.43e-02	7.13e-03	1.08e-03
	order	2.22	2.30	3.02	2.72

Table 4: Convergence rate for the L_2 -error of the RCS for the 2nd and 3rd order effective boundary conditions (EBC) for the elliptic cylinder. Conditions are the same as in Fig. 6.

We consider the same examples as in the above and fix the physical dimensions of the smooth scatterer while the frequency of the incident wave is changed. In Fig. 7 we show the accuracy of the approximation for both 2nd and 3rd order effective boundary conditions for the cylindrical and elliptic case. The general trends are the same in both cases. For increasing frequency, the layer gets electrically thicker and the accuracy of the thin layer approximation deteriorates as one would expect. Extensive numerical tests show that when the coating gets close to one wavelength thick, the approximation slowly fails. However, in that limit, the layer is no longer electrically thin and poses much less of a computational bottleneck.

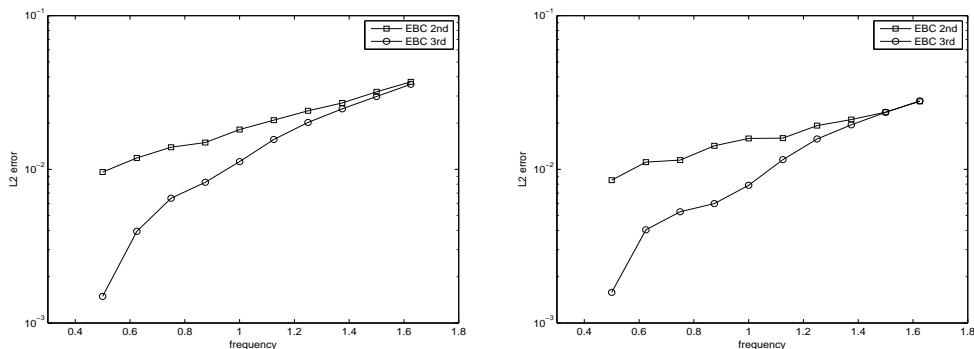


Figure 7: L_2 -errors for the RCS versus normalized frequency of incident waves for the circular cylinder (left) and the elliptic cylinder (right) using 2nd and 3rd order effective boundary conditions. The material coefficients for the thin coating are $\epsilon^\eta = 2.25$ and the thickness is 0.08

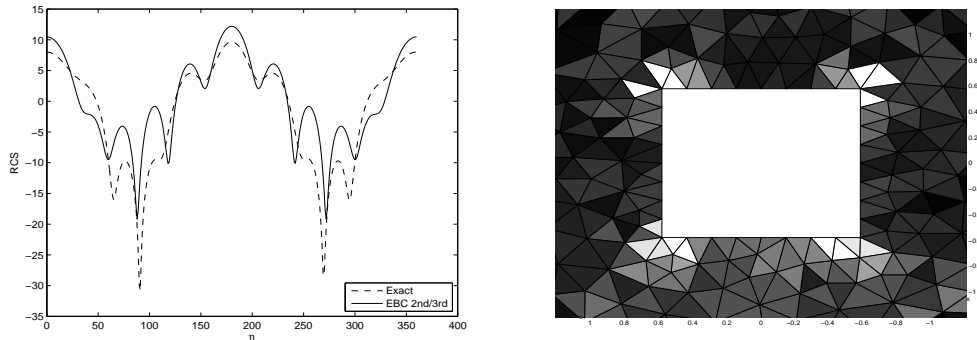


Figure 8: Radar cross section of the brute-force computation (dashed line) and 2nd order effective boundary condition (solid line) on a rectangular cylinder on the left. On the right, we show the distribution of the error of E when the thin layer with thickness $\eta = 0.08\lambda$ consists of an isotropic material with $\varepsilon^\eta = 2.25$. The brighter the area is, the higher the local error is. The brightest color corresponds to the magnitude of 0.8 and the darkest is close to zero.

Figure 7 shows another interesting difference between the two formulations. Recall that the 3rd order conditions depend on the geometric parameters such as the curvature tensor (\mathcal{C}) and the mean curvature (\mathcal{H}), while the 2nd order condition neglects this information. As we have discussed previously, when the boundary is plane, the two conditions are equivalent. However, for the examples considered here, we see a dramatic difference when the frequency of the illuminating wave is decreased while in the high-frequency limit the two schemes behave in similar ways. In the latter case, the curvature over a wavelength is very small and the two schemes behave as if the boundary is approximately plane. In the other limit, however, the curvature of the boundary over a wavelength is much more pronounced and including it in the effective boundary condition improves the accuracy of the results significantly.

5.3 Extension to objects with a non-smooth boundary

The effective boundary conditions are derived under the assumption that the metallic backing is smooth, although, in contrast to most alternatives, the formulation does allow for high curvature. However, for many applications, corners and edges introduce points where the smoothness assumption breaks down and the rigor of the derivation of the models must be relaxed. It is of considerable interest to explore the performance of the effective boundary conditions in this case also to gauge the impact of this violation of the smoothness assumption.

In Fig. 8, we show the difference in the RCS for an infinite cylinder with a square cross section and a thin coating of isotropic material of thickness. Since the cylinder has plane sides, the 2nd and 3rd order scheme are equivalent and

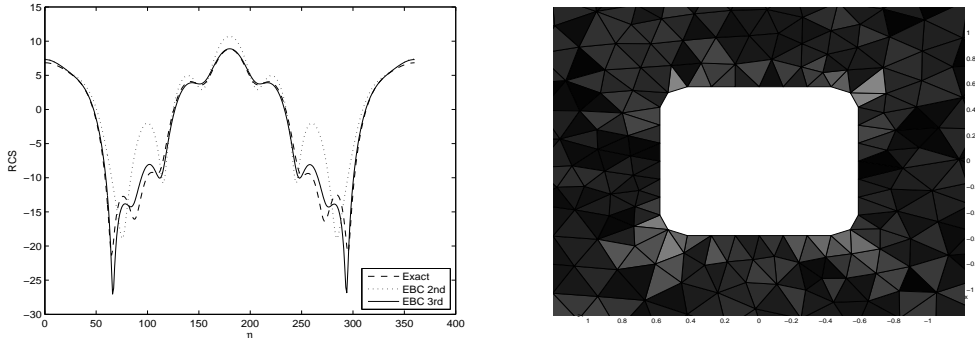


Figure 9: Radar cross section of the brute-force computation (dashed line) and 2nd order (dotted line) and the 3rd order (solid line) effective boundary condition on a smoothed rectangular cylinder with smoothed corners shown on the left. On the right we show the distribution of the error of E when the thin layer with thickness $\eta = 0.08\lambda$ consists of an isotropic material with $\varepsilon^\eta = 2.25$. The same scaling on color as in Fig. 8 is used for comparison

the difference between the brute-force computation and the results using the effective boundary conditions can only be attributed to the difficulty of dealing with nonsmooth boundaries. Another violation results from the observation that when the boundary of the object contains singular points, the thickness of the thin layer has to vary at those points, i.e., the thickness can not be constant on all of Γ . This is further illustrated in Fig. 8 where the difference between the brute-force computation and the thin layer approximation clearly highlights the regions with the corners as the main regions of error.

One way to address this problem is to take advantage of the ability of the effective boundary conditions to handle smooth regions of high curvature and simply substitute the singular points by geometrically similar, but smooth surfaces. For example, for the vertices of the rectangle, one can smoothen them out into small rounded corner. In Figs. 9 and 10, we illustrate the result of this approach for the problem consider in Fig. 8. As expected, the 3rd order condition is now clearly superior to the 2nd order condition due to the area of high curvature being introduced. However, the overall improvement in the agreement of the RCS is rather dramatic and key measures such as the back-and forward scattering is now in agreement with the brute-force results.

It should be noted that the test in Fig. 8 is a severe challenge to the effective boundary conditions due to the small electric size of the square. For electrically larger problems where the separation between the non-smooth points is larger, the impact of these on the performance of the thin layer models is dramatically reduced.

Also, Fig. 11 shows that the RCS of the thin layer approximation of the smoothed rectangular cylinder converges to the RCS of the exact computation

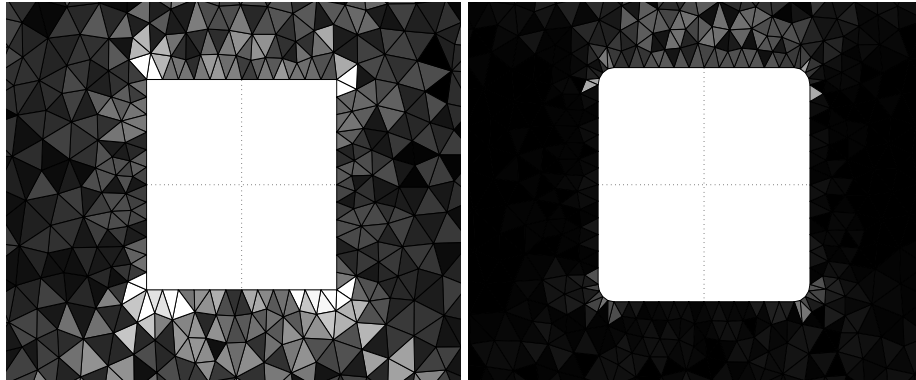


Figure 10: Distribution of error of E when the size of rectangular cylinder (left) and smoothed rectangular cylinder (right) are larger (width and height are 2λ long) are shown. Material properties and the thickness are the same as the previous case. The maximum error of rectangular cylinder is around 1.5 and smoothed cylinder is 0.3 when $T = 5\pi$

of the rectangular cylinder as the radius of small circles at the vertex decreases. In other words, the regularized problem converges to the original problem.

6 Remarks and extensions

We have continued the development of a new family of high-order accurate thin layer models, first proposed in [2] for isotropic materials, for time-domain electromagnetics and discussed its implementation in a discontinuous Galerkin scheme. This allows us to validate the schemes for both one- and two-dimensional cases and to extend the formulation to certain anisotropic materials. The tests confirm design order accuracy and the significant advantages in terms of computational efficiency and overall accuracy of using a high-order effective boundary conditions. This is found to be particularly true for problem with high curvature and low frequency problems.

While the analysis only covers the case of smooth metallic coated objects, we pursued the extension to non-smooth scatterers by computational means and showed that it is reasonable, with minor modifications, to expect good accuracy also in this case.

In this work, we have discussed general but homogeneous layers. However, the extension of the isotropic case to multi-layered coatings is outlined in [2] and the generalization of the methods discussed here to anisotropic coatings can be achieved following the same approach as for the isotropic case.

In part two of this work, we shall discuss a more extensive generalization to include transmission layers and high-order effective boundary conditions for such cases where both reflection and transmission has to be dealt with accurately.

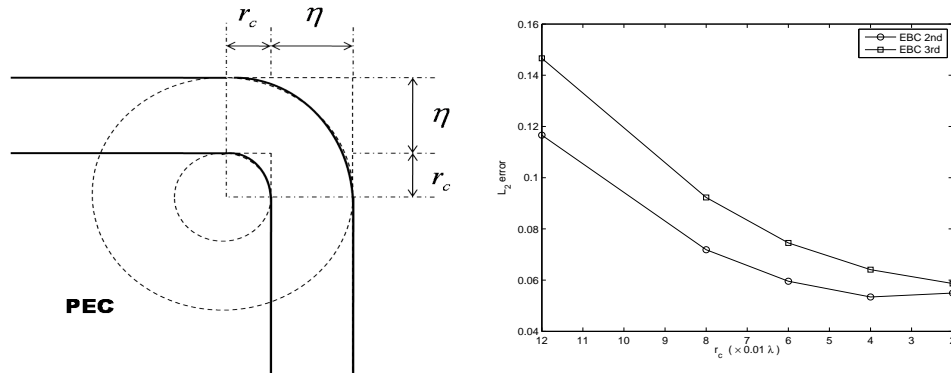


Figure 11: Construction of smoothed rectangular cylinder (left) and RCS errors between the exact computation of rectangular cylinder and the EBC 2nd (circle)/EBC 3rd (rectangle) approximation of smoothed rectangular cylinder (right) are shown. As the radius of circle r_c decreases, the RCS of smoothed rectangular cylinder by thin layer approximation converges to the RCS of the original rectangular cylinder by the exact computation.

Acknowledgements

This work was supported by the U.S. Air Force Office of Scientific Research under the grant FA9550-04-1-0359 and by the National Science Foundation under grants INT-0307475 and CNS-0325110.

References

- [1] S.M. Rytov. Calcul du skin-effet par la methode des perturbations .*J. Phys. USSR. 2, 233-242 (1940).*
- [2] H. Haddar, P. Joly. Stability of thin layer approximation of electromagnetic waves scattering by linear and nonlinear coatings. *J. Comp. Appl. Math. 143 201-236 (2002).*
- [3] J. S. Hesthaven and T. Warburton. Nodal High-Order Methods on Unstructured Grids. *J. Comp. Phys. 181, 186-221 (2002).*
- [4] A. Taflove, Susan C. Hagness. Computational Electrodynamics, The finite-difference time-domain method, Third Edition. *Artech House, Boston (2005).*
- [5] J. S. Hesthaven and T. Warburton. Nodal Discontinuous Galerkin Methods. Algorithms, Analysis, and Applications. *Springer Texts in Applied Mathematics, 54, Springer Verlag, New York (2007).*

- [6] T. B. A. Senior and John L. Volakis. Approximate Boundary Conditions in Electromagnetics. *Institution of Electrical Engineers, New York and London (1995)*.